EFDA–JET–PR(13)08

V.G. Kiptily, S.E. Sharapov, T. Gassner, C. Perez von Thun, S.D. Pinches, D.B. Alper, F.E. Cecil, D. Darrow, V. Goloborod'ko, C. Hellesen, J. Mailloux, A.W. Morris, V. Yavorskij and JET EFDA contributors

Study of Interaction Between Fast Ions and MHD Instabilities by Fusion Product Measurements in Joint European Torus

"This document is intended for publication in the open literature. It is made available on the understanding that it may not be further circulated and extracts or references may not be published prior to publication of the original when applicable, or without the consent of the Publications Officer, EFDA, Culham Science Centre, Abingdon, Oxon, OX14 3DB, UK."

"Enquiries about Copyright and reproduction should be addressed to the Publications Officer, EFDA, Culham Science Centre, Abingdon, Oxon, OX14 3DB, UK."

The contents of this preprint and all other JET EFDA Preprints and Conference Papers are available to view online free at www.iop.org/Jet. This site has full search facilities and e-mail alert options. The diagrams contained within the PDFs on this site are hyperlinked from the year 1996 onwards.

Study of Interaction Between Fast Ions and MHD Instabilities by Fusion Product Measurements in Joint European Torus

V.G. Kiptily[1], S.E. Sharapov[1], T. Gassner[2],C. Perez von Thun[3,4], S.D. Pinches[5], D.B. Alper[1], F.E. Cecil[6], D. Darrow[7],V. Goloborod'ko[2,8], C. Hellesen[9], J. Mailloux[1], A.W. Morris[1],V. Yavorskij[2,8],and JET EFDA contributors*

JET-EFDA, Culham Science Centre, OX14 3DB, Abingdon, UK

[1]EURATOM-CCFE Fusion Association, Culham Science Centre, OX14 3DB, Abingdon, OXON, UK
[2]EURATOM/OEAW Association, ITP, University of Innsbruck, Austria
[3]JET-EFDA Close Support Unit, Culham Science Centre, Abingdon, United Kingdom
[4]Max-Planck-Institut f˙ur Plasmaphysik, EURATOM-Association IPP, Garching, Germany
[5]ITER Organization, Route de Vinon-sur-Verdon, 13115 St. Paul-lez-Durance, France
[6]Colorado School of Mines, 1500 Illinois Street, Golden, Colorado, USA
[7]Princeton Plasma Physics Laboratory, Princeton, New Jersey, USA
[8]Institute for Nuclear Research, Kiev, Ukraine
[9]Department of Physics and Astronomy, Uppsala University, BOX 516, Uppsala, Sweden
** See annex of F. Romanelli et al, "Overview of JET Results", (24th IAEA Fusion Energy Conference, San Diego, USA (2012)).*

Preprint of Paper to be submitted for publication in
The Japan Society of Plasma and Nuclear Fusion Research

ABSTRACT.

Fast ion redistribution and losses caused by plasma disruptions, Toroidal Alfvén Eigenmodes (TAE) and fishbones are measured with a suite of improved gamma-ray diagnostics, Neutral Particle Analyser (NPA), neutron spectrometry, Faraday Cups and a Scintillator Probe (SP). Fast ion populations in the MeV energy range were generated in fusion reactions and were also produced by 3rd harmonic Ion Cyclotron Resonance Heating (ICRH). Significant fast ion losses preceding plasma disruptions were often detected by SP in discharges with high β_N. These losses were caused by the m = 2/n = 1 kink mode and typically occurred at the time of thermal quench, before the current quench. Core-localised TAE modes inside the q = 1 radius causing redistribution of the fast ions in the resonance energy range were directly measured for the first time with the gamma-ray camera, confirming that the TAE instability expels fast ions from inside the q = 1 radius and triggers the monster sawtooth crashes. Energy and pitch angle resolved SP measurements of lost fusion products in the MeV energy range were found to correlate with low-frequency fishbone oscillations driven by 100keV beam ions. The origin and amplitude of these nonresonant losses are investigated.

1. INTRODUCTION

This paper summarises results of studies of fast ion losses caused by plasma disruptions, TAE and fishbones in JET plasmas with a carbon wall using the improved diagnostic capability built up on JET in recent years [1]. Understanding physics of fast ions will play a crucial role in the design of plasma facing components for DEMO and for operation of ITER.

Diagnostics of the confined ions, i.e. gamma-ray diagnostics [2,3], neutral particle analyser (NPA) [4], neutron spectrometry with TOFOR [5], as well as the diagnostics of lost ions, Faraday Cups [6] and Scintillator Probe (SP) [7], were all used for simultaneous measurements of various species of ions in the MeV energy range in D-D, D-3He, and D-4He plasmas.

The high time resolution of diagnostics allowed the measurements of both resonant (interaction with TAE) and abrupt non-resonant (disruptions) MHD effects of the redistribution and losses of energetic ions. The fast ion populations were generated in fusion reactions $D + D \rightarrow p(3MeV) + T(1MeV)$, $D + D \rightarrow {}^3He(0.82MeV) + n(2.45MeV)$ and $D + {}^3He \rightarrow \alpha(3.6MeV) + p(14.7MeV)$, and were also produced by Neutral Beam Injection (NBI) and by accelerating minority-ions or NBIions with ICRH. The losses from the three main types of MHD instabilities are described in turn, providing an overview of recent work as well as new results.

2. FAST ION LOSSES AND M=2/N=1 KINK MODE

Fast ion bursting losses preceding a plasma crash or disruption were detected by the SP in Advanced Tokamak (AT) plasma discharges with high β_N and q(0)>1.5 [8]. The m = 2/n = 1 infernal kink modes and m = 3/n = 2 Neoclassical Tearing Modes (NTMs) were dominantly limiting the plasma performance in these experiments. The most significant MHD impact on the plasma was observed where the m = 2/n = 1 modes had high amplitude. Significant losses of fast ions in the MeV range

accelerated with ICRH and fusion products were detected with the SP diagnostic during plasma disruptions caused by such high-amplitude modes.

The scintillator probe, which is located just below the mid-plane of the JET torus outside the plasma, detects lost ions and provides information on the lost ion pitch angle $S = \arccos(v_{||}/v)$ with 5% resolution in the range 35° – 85° and gyro-radius between 3cm and 14cm with 15% resolution. The basic principle of scintillator measurements is the emission of light by a scintillating material after a fast ion strikes this material. Selection criteria for the particles that hit the scintillator are introduced by using a collimator matched to the equilibrium magnetic field of JET. An optical arrangement within the scintillator probe is used to transfer the light emitted by the scintillator through a coherent fibre bundle towards a charge-coupled device (CCD) camera and a photomultiplier (PMT) 4×4 array. The CCD camera used in SP can provide 10–50ms snapshots of the light intensity on the pitch-angle – gyro-radius grid calculated with the EfipDesign code [9]. The PMT current was digitized with 5kHz (200 Os time bins), however the characteristic scintillator decay time is 2ms.

Figure 1 shows time traces of electron temperature, the n = 1 MHD signal, internal plasma inductance, plasma current, toroidal rotation and fast ion losses measured with a PMT array observing the scintillator plate for two Pulse No's: 77894 and 77896 with a weak internal transport barrier.

In these discharges, with 21MW NBI, 7MW ICRH (H-minority heating) and 2.5MW Low Hybrid Current Drive (LHCD), although MHD activity appeared to have similar features in the magnetic spectrograms (see Fig.2) quite different consequences resulted depending on their amplitudes. Whilst in the first discharge (Pulse No: 77894) one can see a fast drop of T_e associated with the MHD event, a similar MHD instability initiates a thermal quench in the second discharge, with a disruption to follow.

A theory of fast ion redistribution due to the m = 2/n = 1 instability was developed in Ref.10, where the interaction mechanism of energetic trapped ions with the pressure driven MHD instability (similar to that shown in Fig.1) was studied, but without SP data. In the case of the discharge with a disruption (Pulse No: 77896), the internal inductance and plasma rotation are dropping similar to a JET pulse discussed in [10] just before the thermal quench. In the Pulse No: 77894 the plasma rotation also decreases but an increase in the inductance is observed. One notes that in Pulse No: 77894 the plasma rotation significantly decreased off axis at R = 3.3–3.4m during the crash (t_{cr} = 5.533s), while a central plasma rotation drop was observed in the case of Pulse No: 77896 (t_{cr} = 5.485s). Figure 3 demonstrates how the electron temperature profile reacts to the MHD events in these two different discharges, with the mode at the q = 2 magnetic surface seen from the electron temperature profiles.

There is no evidence provided by the γ-ray spectrometers that the D-beam ions were also accelerated by ICRH (i.e. γ-ray emission from the $^{12}C(D,p\gamma)^{13}C$ reaction was not detected [2]). This is interpreted as the SP signal being from H-ions alone accelerated with ICRH.

The detected lost ions are most likely lost due to the changes in the Larmor radius or the pitch angle of confined ions. The losses observed in the quiescent period before the mode in Pulse No:

77894 at t = 5.475s are localised mainly in the vicinity of the trapped-passing boundary region of phase space. Similar losses are seen in plasmas without MHD, such as the losses at t = 5.425s in Pulse No: 77896. The footprints of losses at t = 5.525s (Pulse No: 77894) and t = 5.475 (Pulse No: 77896) cover both the crash (Pulse No: 77894) and the whole disruption period (Pulse No: 77896). The saturation of the MHD signal in Fig.1 prevents the investigation of the loss in intensity as function of the mode amplitude in this case. However the temporal evolution of the losses detected by SP shows the phase space of the losses moves notably during the MHD event. During the crash in Pulse No: 77894 the main losses are around the pitch angle of H ions resonating with ICRH, deep in the trapped particle region of the phase space: the pitch-angle of the maximum loss is on the red line marking the ICRH resonance position on the SP grid in Fig.4. The pitch-angles of resonant H ions detected by SP lie at the pitch angle $\theta \cong \arccos(1-R_{res}/R_{SP})^{1/2} = 60^{o}$, with $R_{res} \cong 2.90$m and RSP = 3.82m corresponding to the major radii of the resonance and the scintillator probe. For the disruption in Pulse No: 77896 a similar trend is seen, but the loss region is expanded and the magnitude of losses is much higher, due to a much larger amplitude of the MHD instability and perhaps a more complex magnetic structure. After the event in Pulse No: 77894, the quiescent losses are reduced (Fig 4 (a), 3rd frame), suggesting the fast ion population has been significantly depleted.

The orbits of lost H-ions calculated backwards in time from the different hot spot coordinates, (9cm, 57^{o}), (9cm, 58^{o}) and (7cm, 59.5^{o}) of the SP are presented in Fig.5. These calculations were made without taking into account the MHD perturbations, which could pitch angle scatter the H-ions. These orbits vary from the marginally passing to trapped ones.

3. FAST ION INTERACTION WITH TORNADO MODES

A set of experiments were carried out where interactions of core-localised TAE modes [11, 12], so-called 'tornado' modes localised inside the q = 1 magnetic surface, with fast D-ions in the MeV energy range were studied in plasmas with monster sawteeth.

The tornado modes were identified as core-localized TAEs within the q = 1 radius [13]. The effect of tornado modes on fast particles was first detected on JT-60U [11], where a significant loss of the fast-ion confinement and degradation of total plasma energy content were observed.

Also TAE and tornado mode activities affecting fast ion power deposition profiles were found on DIII-D [14, 15] and on TFTR [16]. The fast particle redistribution/ losses similar to those observed on JT-60U were found on JET as a significant (by a factor of 2) decrease of γ-ray emission coming from the nuclear reaction $^{12}C(p,p'\gamma)^{12}C$ during the combined activity of tornado modes (inside the q = 1 radius) and TAE (outside the q = 1 radius) [17,18]. Also core-localized TAE modes were observed to cause significant fast ion redistribution in the plasma core and enhanced losses in AT plasma discharges [19]. This is a resonant process, and it is estimated that deuterons with energy ~0.5MeV are resonant with the tornado modes. For the first time, JET has performed experiments in which the resonant redistribution of D ions could be directly observed with the 2D gamma-ray camera [3].

In the present experiments a population of the fast particles was obtained by central 3rd harmonic ICRH-acceleration of D-beam ions in the D-plasma. Figure 6 shows wave-forms of a typical plasma discharge with a monster sawtooth. Figure 7 shows many discrete modes in the TAE frequency range. Just before the crash, at t>15.1 sec TAE and bi-directional tornado modes are seen with toroidal mode numbers n = 3, ± 4, ± 5, 6, 7, 8. The existence of the n = 3 mode, the lowest-n mode before the monster sawtooth crash, shows that q (0) at the time of the mode appearance, 15.1sec, has to be below $q_{TAE}^{n=3} < 0.83$, which is the existence condition, $q_{TAE}^{n=3} = (2m + 1)/2n$, for n = 3.

The γ-ray emission from the reaction $^{12}C(D,p\gamma)^{13}C$ was observed in these experiments indicating that the ICRH power was absorbed by deuterons and the D-ions were accelerated. In the $^{12}C(D,p\gamma)^{13}C$ reaction, the deuterons interact with ^{12}C to yield ^{13}C in excited states with the energies 3.09MeV, 3.68MeV and 3.85MeV. Observation of the γ-rays de-exciting these levels requires necessarily deuterons with energies exceeding 0.5MeV. However, those deuterons with energies close to the resonance energies of 0.9MeV, 1.9MeV and 2.5MeV provide the main contribution to the gamma-line intensity. Gamma-ray energy spectra were measured with two independent devices, one with a horizontal (BGO scintillation detector) and one with a vertical line of sight (NaI scintillation detector) through the plasma centre [2]. In order to reduce the neutron flux and the γ-ray background polythene attenuators are used. The γ-rays are continuously recorded in all discharges over the energy range 1-28MeV, with an energy resolution of about 3-4% at 10MeV and time-resolution up 1 ms depending on the count rate. The γ-ray spectrum measured with a horizontal detector is presented in Fig.8. A peak at 3.09MeV (transition $3.09 \rightarrow 0$) and a peak, which is a superposition of the 3.68MeV (transition $3.68 \rightarrow 0$) and 3.85MeV (transition $3.85 \rightarrow 0$) peaks reflects the presence in the plasma of the fast Dions with $E_D > 0.5$MeV.

Spatial profiles of the γ-ray emission in the energy range $E_\gamma > 1$MeV were measured using the 2D γ-ray camera [3], which have 10 horizontal and 9 vertical collimated lines of sight. Each collimator defines a poloidal-viewing extent at the centre of plasma of about 10cm. The detector array is comprised of 19 CsI photo-diodes. These detectors are well calibrated with radioactive sources ^{22}Na (0.511MeV, 1.275MeV), which are embedded in the detector-array module, and with 4.44 MeV gammas generated by the Am-Be neutron source. The data acquisition system accommodates the γ-ray count-rate measurement in 4 independently adjustable energy windows. This allows γ-ray peaks for a given fast ion population in specific windows to be counted separately. The measured line-integral γ-ray brightness along the viewing direction can be tomographically reconstructed to get the local γ-ray emissivity in a poloidal cross-section, assuming that the distribution of the low-Z impurities is uniform in the plasma core as confirmed by atomic spectroscopy measurements. The effective spatial resolution of the diagnostic in these experiments is about ±6cm. The special energy window (see Fig.8), containing the 3.09MeV peak with its single and double escape satellites was set up to measure spatial profiles of the γ-ray emission from D ions. Another energy window related to the neutron induced γ-ray emission was used for assessments of the background component recorded in the 3.09MeV window.

Measurements of confined fast particles with the 2D γ-ray camera made it possible to distinguish the energy ranges of fast D-ions using I-ray emission from the $^{12}C(D,p\gamma)^{13}C$ reaction threshold deuteron energy $E_D \approx 0.5$MeV [3], a much lower threshold than the 4.5MeV proton threshold of the $^{12}C(p,p'\gamma)^{12}C$ reaction in [17,18]. In addition DD neutron data from the TOFOR provides information on high energy deuterons $E_D > 0.5$MeV [5]. This makes it possible to observe their spatial redistribution during the core-localised TAE activity preceding monster sawtooth crashes.

In all discharges with tornado modes an extensive re-distribution of fast D-ions in the energy range of 0.8MeV–1.2MeV was observed with the 2-D γ-camera. Indeed, line-integrated emissivities of 3.09-MeV γ-rays from the $^{12}C(D,p\gamma)^{13}C$ reaction depicted in Fig.9 show that intensities of central channels of the vertical camera (#15 and #16) begin to slowly decrease with the appearance of tornado modes during the monster sawtooth period. At the same time, intensities of the high- and low-field side channels (#14, #17 and #18) are growing. That means the energetic particles are leaving the plasma centre and moving toward the periphery. The lines of sight for neutron and γ-spectrometers are relatively narrow and are overlapping with γ-ray camera channels #14, #15 and ch#16. Tomographic reconstruction of the line-integrated 3.09MeV γ-ray intensities measured with 2-D γ-camera are presented in Fig.10. The left figure shows the emissivity profile related to the period without TAE modes. The right shows the profile observed during the TAE activity that demonstrates the redistribution of fast D-ions.

Neutron and γ-ray spectrometry have also provided evidence of the D-ion redistribution [5]. It was found that intensity of DD-neutrons with energy $E_n > 4.5$ MeV produced by ions with $E_D > 1.3$ MeV is decreasing in the period of the tornado mode development. The same tendency has been observed for 3.1MeV gammas from the $^{12}C(D,p\gamma)^{13}C$ reaction measured with NaI detector in the TOFOR field of view. It is important to emphasize that charge-exchange diagnostics did not indicate changes in the carbon concentration in the period 13–15s in this discharge.

One can see from Fig.7 that at around t = 15.5s the observed TAE activity is abruptly terminated by the occurrence of a monster sawtooth crash, which may have been triggered by the loss of fast ion stabilization due to the tornado modes [14–18]. A burst of fast ion losses during the sawtooth crash is clearly seen in Fig.6. The change in the equilibrium profiles, as a result of the sawtooth crash, most notably for the safety factor, q, then violates the existence criterion for the tornado modes which accounts for their abrupt disappearance. The modelling of D-ion redistribution [20] in the presence of tornado modes has been carried out with HAGIS [21] using HELENA [22] equilibrium and TAE modes calculated using the CASTOR code [23].

4. FISHBONE EFFECTS ON FAST ION LOSSES

High-β NBI-driven poloidal magnetic field oscillations in tokamak plasmas in the frequency range ~ 10-20kHz are destabilised with perpendicular and tangential neutral beams and associated with redistribution of the beam ions [24, 25]. Trapped and circulating beam-ions resonate with the core-localised m = 1/n = 1 mode [26]. Drops in the neutron rate dominated by beam-plasma DD reactions

of up to 10% are associated with this activity in JET plasmas [27].

Interaction of fusion-born α-particles with fishbones is one of the important issues for burning plasmas in ITER-type machines. Estimates show that fishbones may be driven by resonant interaction with relatively low-energy alphas, $E \cong 400$keV. For this energy range, any radial transport of the almost thermalised alphas caused by the fishbones may become beneficial since it helps to solve the ash removal problem. However, the low-frequency fishbone driven by thermalised alphas may also degrade the confinement of alphas at much higher energies. This question was discussed in [28], and it was shown that the loss of toroidal symmetry caused by the $m = 1/n = 1$ perturbation may indeed strongly affect the highly energetic non-resonant alphas. In order to validate the theory of the non-resonant losses, JET experiments were performed by measuring losses of highly energetic ions in the MeV energy range in the presence of fishbones driven by NBI ions with energy 80–100 keV. Namely, the energy and pitch angle resolved SP measurements of MeV-ions ejected from the plasma during the non-resonant fishbone oscillations were studied [29]. The lost ions are identified as fast protons accelerated by ICRH (~0.5-4MeV). Losses arriving at the probe are enhanced by about a factor 10-20 with respect to MHD-quiescent levels and are found to increase quadratically with the fishbone amplitude. Numerical simulations have been performed which combine the HAGIS, MISHKA and SELFO codes [30]. The losses are found to originate from orbit stochastic diffusion of trapped protons near the plasma boundary or/and from counter-passing protons deep in the plasma core which transit under the influence of the fishbone into an unconfined trapped orbit. The simulations show that the losses are of non-resonant type indeed confirming the mechanism proposed in [28] for highly energetic C-particles.

CONCLUSIONS

In JET discharges with high β_N and $q(0)>1.5$, the $m = 2/n = 1$ kink modes which limit the plasma performance were also found to affect strongly the losses of ICRH-accelerated energetic ions. These losses exhibit a bursting temporal evolution and achieve peak values (as measured at the SP position) up to factor ~20 higher than those in MHD quiescent plasmas. One of the unexpected features for the losses of ICRH accelerated ions during plasma disruptions caused by the kink modes was the preserved pitch-angle distribution of the lost ions. This distribution remained close to the pitch-angle determined by ICRH well after a disruption even though it might be expected that Coulomb collisions could transform the distribution function into an isotropic one. The increase of the losses in amplitude and the narrow pitch-angle of the lost ions may require a further assessment of the impact of such losses on Be walls.

Experiments on beam acceleration with 3rd harmonic ICRH carried out on the JET tokamak provided important new data on monster sawteeth stabilisation by fast ions interacting with tornado modes (TAE inside the $q = 1$ radius). In general, the experimental results show trends expected from theory [14-16], which explains the monster crash as a result of the tornado modes expelling fast ions to the region outside the $q = 1$ radius with the inevitable loss of the fast ion stabilising effect

on the sawtooth. This extends earlier studies of this effect on JET [12, 17, 18], with a different fast ion population (deuterium instead of hydrogen) and new γ-ray data on fast ions with energy ≥ 0.5MeV, which is close to the resonance energy for the ion interaction with tornado modes. This allows one to observe a γ-ray response of fast ions resonating strongly with the tornado modes in the energy range 0.8MeV–1.2MeV inside the q = 1 radius. Together with the neutron spectrometry available for D-D reactions, much better coverage of the fast ion redistribution by the tornado modes was experimentally obtained. These experiments provide a very good foundation for sawtooth and tornado modelling [20]. The experimental observation of the non-resonant losses of trapped energetic ions in the presence of NBI-driven low-frequency fishbones [29] was found to be in line with theory [28]. This effect could be important for fusion-born alpha-particles in scenarios with fishbones (e.g. hybrid scenarios).

ACKNOWLEDGMENTS.

This work, part-funded by the European Communities under the contract of Association between EURATOM and CCFE, was carried out within the framework of the European Fusion Development Agreement. The views and opinions expressed herein do not necessarily reflect those of the European Commission. This work was also part-funded by the RCUK Energy Programme under grant EP/I501045. The views and opinions expressed herein do not necessarily reflect those of the ITER Organization.

REFERENCES

[1]. Kiptily, V.G. et al., Nuclear Fusion **49** (2009) 065030.
[2]. Kiptily, V.G., et al., Nuclear Fusion **42** (2002) 999.
[3]. Kiptily, V.G., et al., Nuclear Fusion **45** (2005) L21.
[4]. Afanasyev, V. I. et al., Review of Scientific Instruments **74** (2003) 2338.
[5]. Hellsen, C. et al., Nuclear Fusion **50** (2010) 022001.
[6]. Darrow, D. S., et al., Review of Scientific Instruments **75** (2004) 3566.
[7]. Baumel, S., et al., Review of Scientific Instruments **75** (2004) 3563.
[8]. Mailloux, J., et al., in Fusion Energy 2010 (Proc. 23rd Int. Conf. Daejeon, 2010) (Vienna: IAEA) CD-ROM file EXC/1-4 and http://www-naweb.iaea.org/napc/physics/FEC/FEC2010/html/index.htm
[9]. Werner A., Weller A. and Darrow D. S., Review of Scientific Instruments **72** (2001) 780.
[10]. Gorelenkov, N.N. et al., Physics of Plasmas **10** (2003) 713
[11]. Saigusa M. et al., Plasma Physics and Controlled Fusion **40** (1998) 1647
[12]. Sandquist et al., Physics of Plasma **14** (2007) 122506
[13]. Kramer G.J. et al., Physical Review Letters **92** (2004) 015001
[14]. Heidbrink W.W. et al., Nuclear Fusion **39** (1999) 1369
[15]. Bernabei S. et al., Nuclear Fusion **41** (2001) 513

[16]. Bernabei S. et al., Physical Review Letters **84** (2000) 1212
[17]. Pinches S. D. et al., Plasma Physics and Controlled Fusion **46** (2004) B187
[18]. Sharapov S.E. et al., Nuclear Fusion **45** (2005) 1168
[19]. Nabais F. et al., Nuclear Fusion **50** (2010) 084021
[20]. Gassner T. et al., Physics of Plasmas **19** (2012) 032115
[21]. Pinches S.D. et al Computer Physics Communications **111** (1998) 133
[22]. Kerner W. et al 1998 Journal of Computational Physics **142** 271
[23]. Huysmans G.T.A., Goeldbloed J. P., and Kerner W., Proc. CP90 Conf. Computational Physics, Amsterdam, the Netherlands, September 10–13, 1990, p.371, World Scientific Publ. Co.(1991)
[24]. M^{C}Guire K. et al, Physical Review Letters **50** (1983) 891
[25]. Heidbrink W.W. et al, Physical Review Letters **57** (1986) 835
[26]. Coppi, Miglioulo and Porcelli, Physics of Fluids **31** (1988) 1630
[27]. Borba D. et al Nuclear Fusion **40** (2000) 775
[28]. Coppi B., Porcelli F., Fusion Technology **13** (1988) 447
[29]. Perez Von Thun et al., Nuclear Fusion **50** (2010) 084009
[30]. Hedin J. et al., Nuclear Fusion **42** (2002) 52

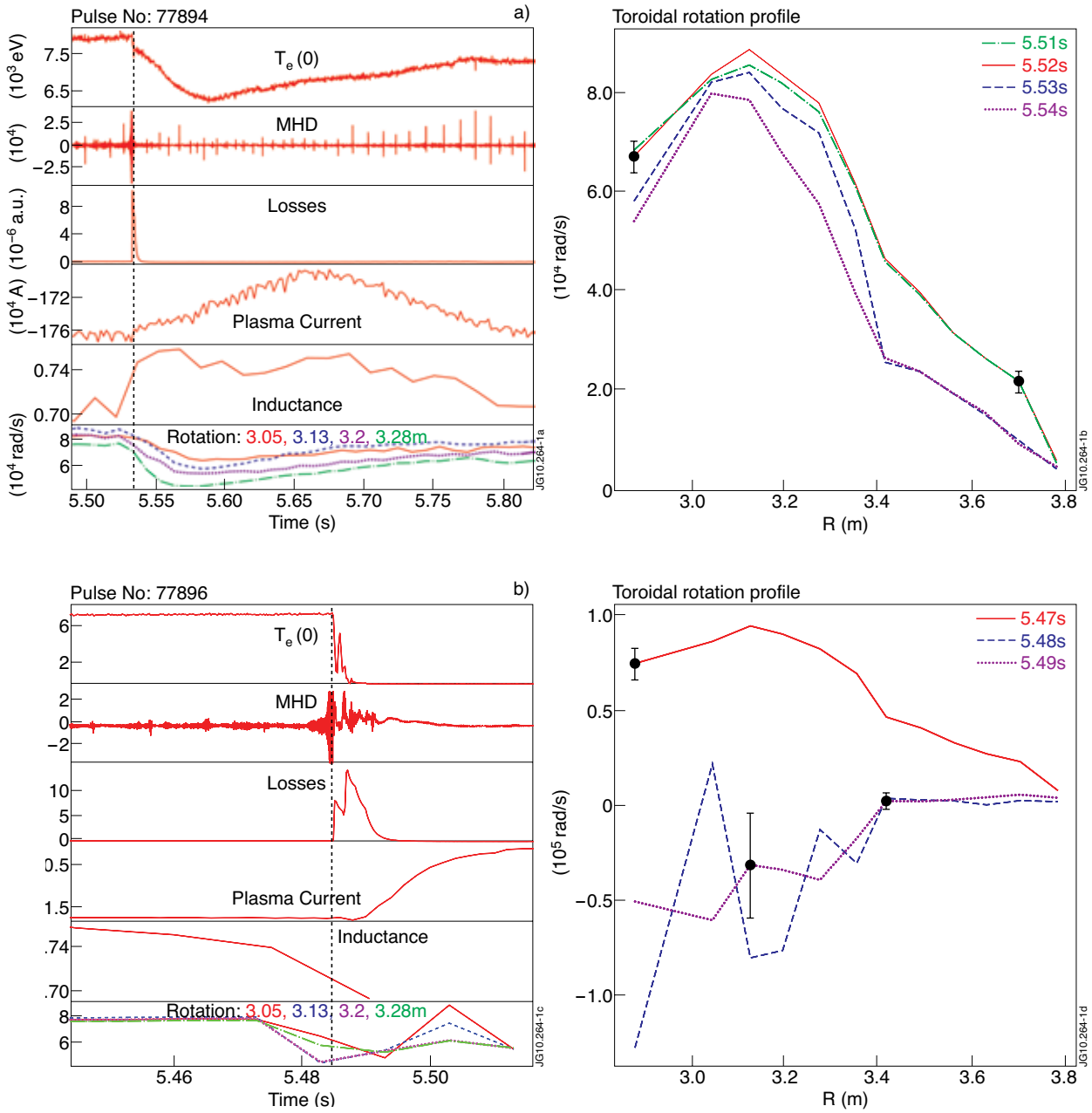

Figure 1: Time-traces of plasma parameters, SP losses and toroidal rotation profiles measured in 2.7T/1.8MA Pulse No's: 77894 (a) and 77896 (b).

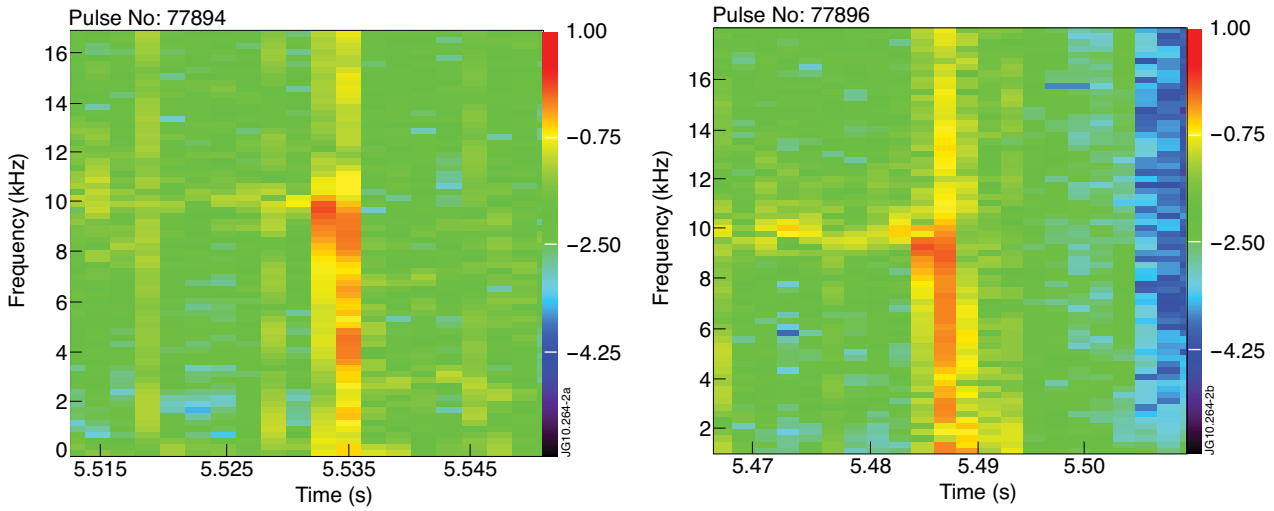

Figure 2: Magnetic spectrograms showing m = 2/n = 1 mode in Pulse No's:77894 and 77896.

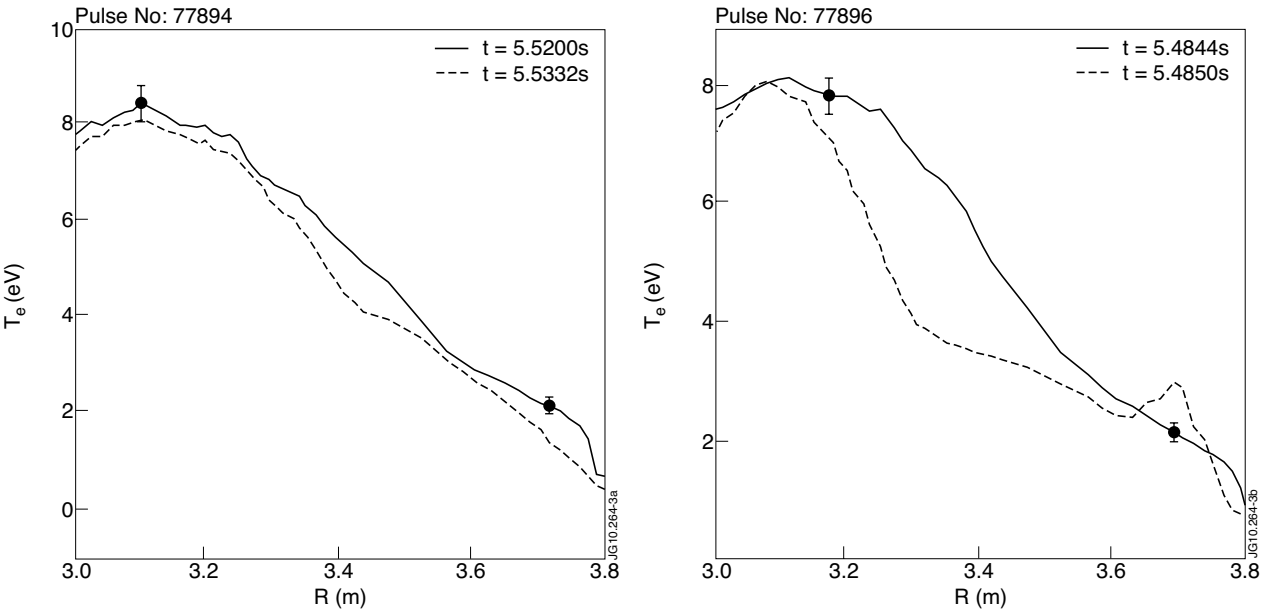

Figure 3: Electron temperature profiles before (solid) and after the crash event (dash) in Pulse No's: 77894 and 77896; before and during MHD q = 2 is located at R = 3.4m in Pulse No: 77894 and R = 3.3m in Pulse No:77896.

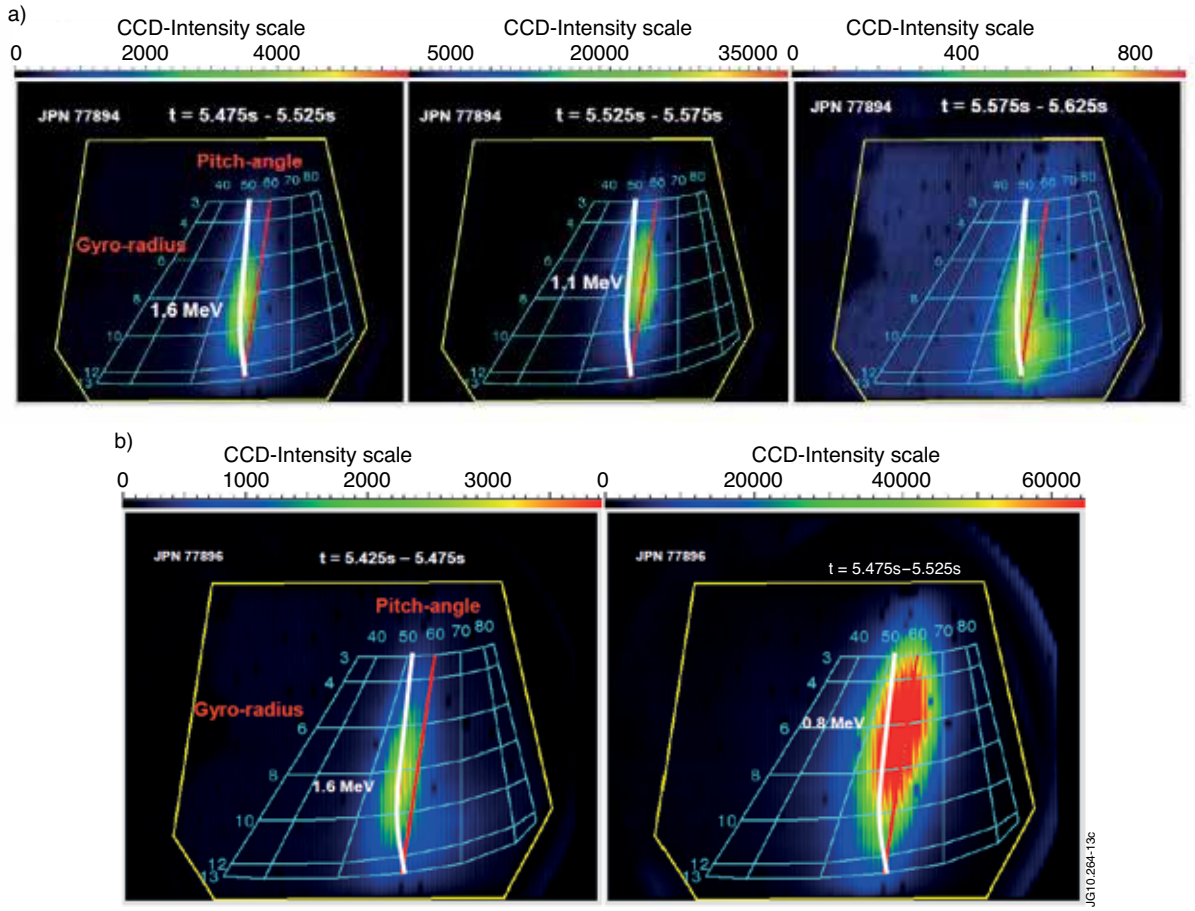

Figure 4: Footprints of losses detected with SP probe: (a) Pulse No: 77894 with crash at t = 5.53s; (b) Pulse No: 77896 ended with disruption at t = 5.486s; exposure of the snapshots – 50ms; red line – pitch-angle of the ICRH resonant ions; white line – the trapped-passing boundary on the SP grid. In (a) and (b) the first footprints related to periods before the crash (Pulse No:77894) and the disruption (Pulse No:77896); massive losses during the crash (second footprint in (a)) and the disruption (second footprint in (b)) are clearly seen. The losses after the crash are shown in (a) third footprint.

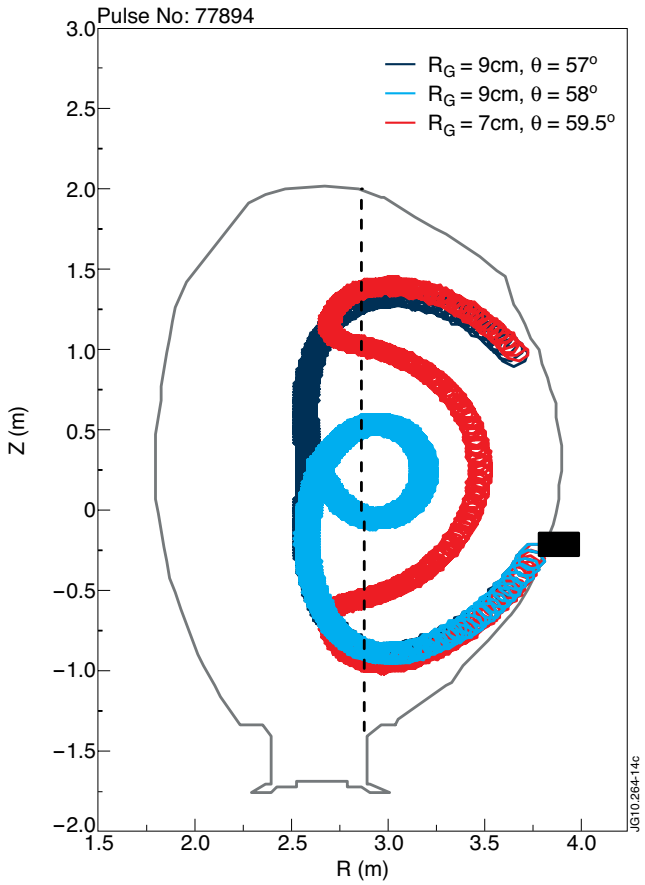

Figure 5: Orbits of lost H-ions calculated backward in time from (RG , S) coordinates on the scintillator related to the loss footprints in the Pulse No: 77894 (see FIG.4a); dash line – position of the resonance layer at 2.66T/1.75MA and f_{ICRH} = 42–42.5MHz.

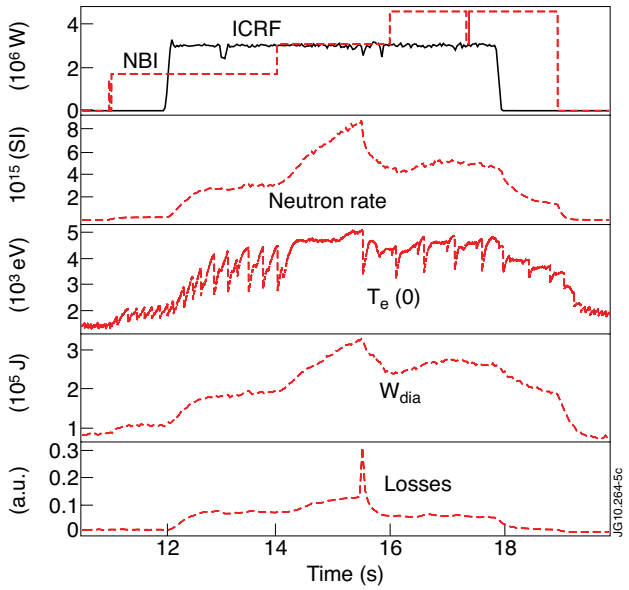

Figure 6: A typical JET D-plasma discharge 2.2T/2.2MA with 3rd harmonic ICRH (51MHz) of D beam-ions.

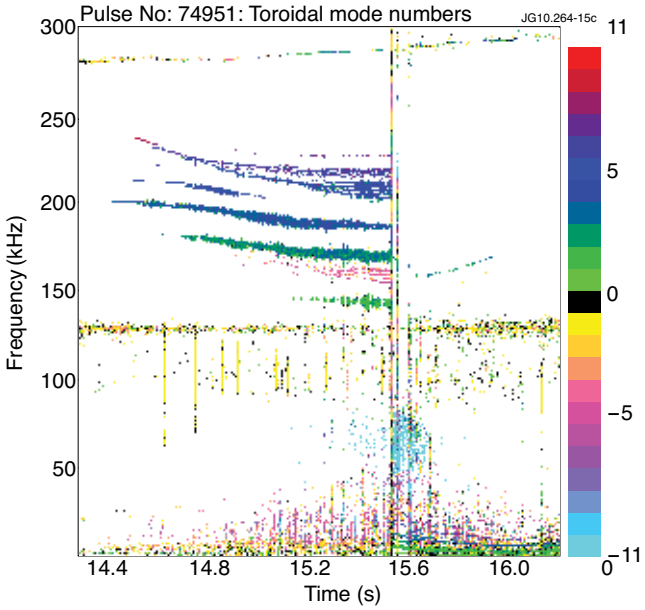

Figure 7: Magnetic spectrogram showing toroidal mode numbers of TAE and tornado modes before monster sawtooth crash in Pulse No:74951.

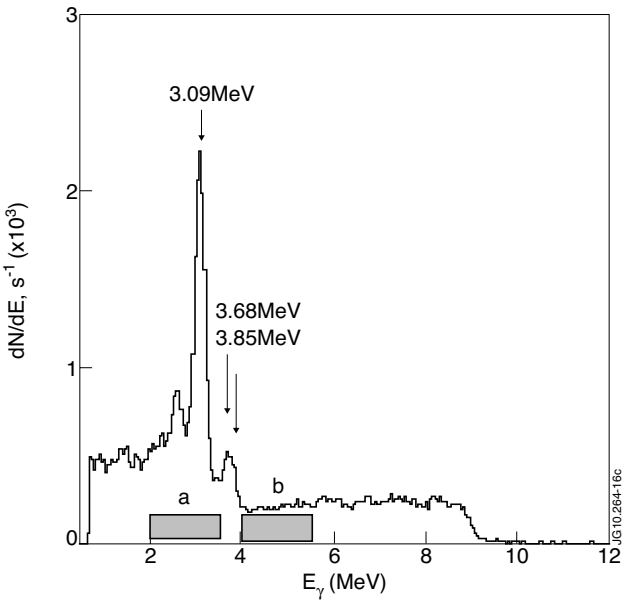

Figure 8: A typical γ-ray spectrum recorded with BGO-detector in these experiments; box (a) shows the energy window, which was set up for intensity measurements of the 3.09MeV gammas; box (b) shows the window used for assessments of γ-ray background emission generated by neutrons.

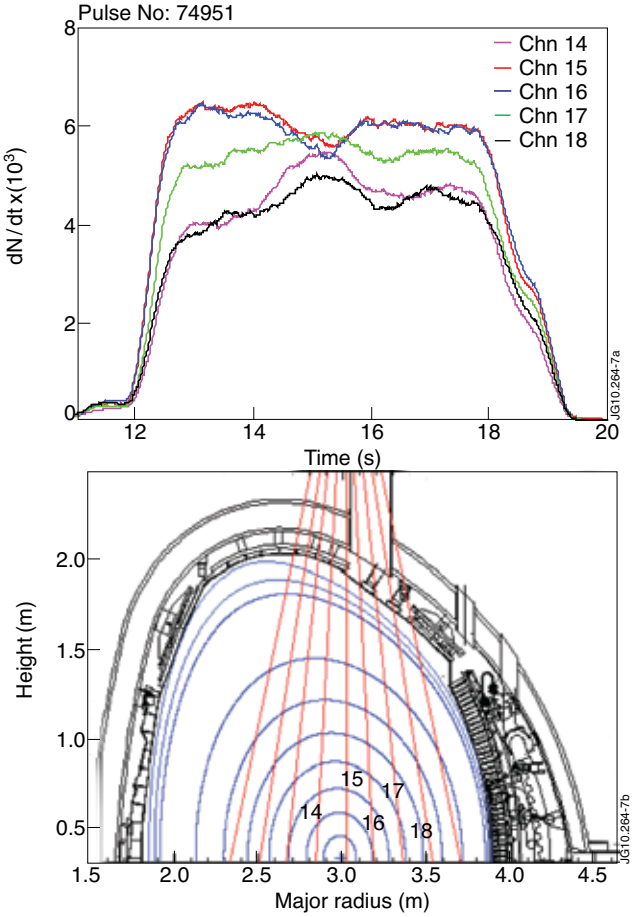

Figure 9: Top: 3.1MeV γ-ray intensities vs. time recorded by vertical camera; bottom – the vertical camera lines of sight.

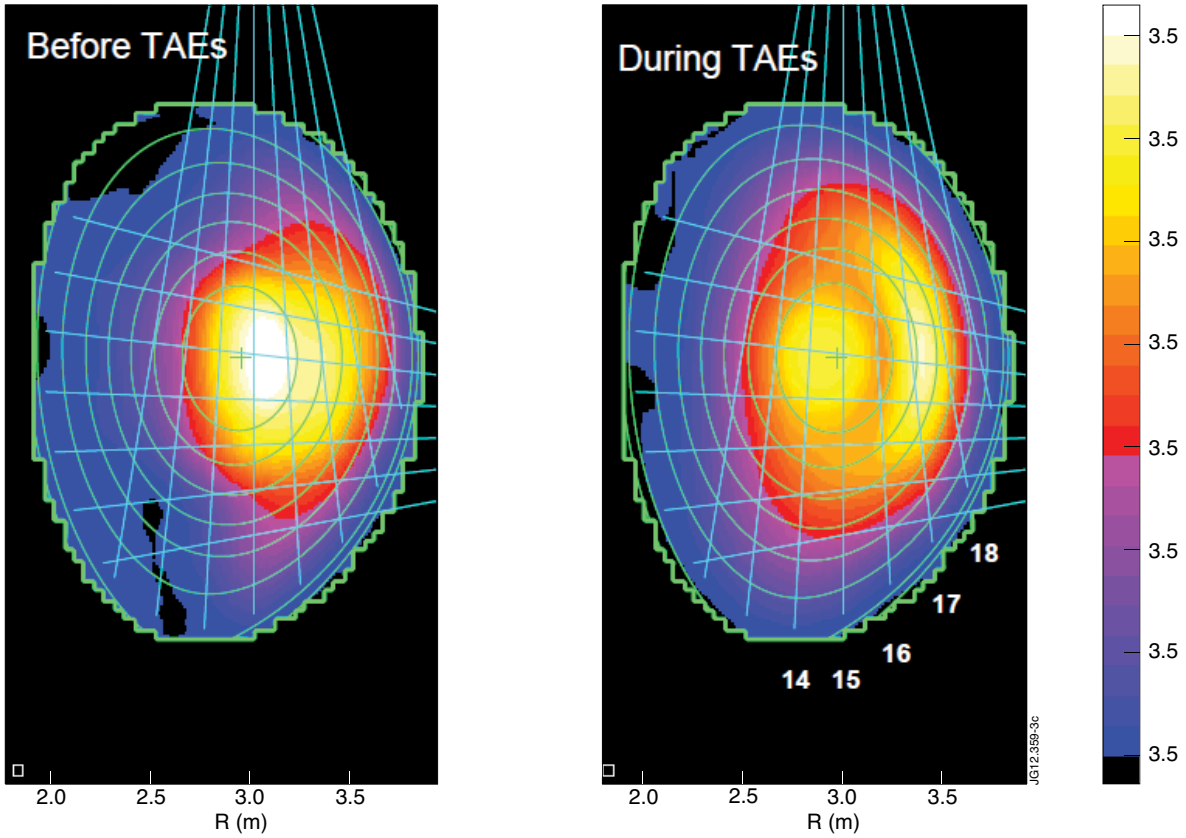

Figure 10: Tomographic reconstruction of the line-integrated 3.09MeV γ-ray intensities measured with gamma cameras: left – the emissivity profile related to the period without TAE modes; right – the profile observed during the TAE activity.